*Sound & Vibration* 2026, 60(4), 4135.
doi: https://doi.org/10.59400/sv4135

Article

# Research on fatigue life calculation method of droppers in high-speed railway catenary

**Hongbo Kou[1], Yongming Yao[1,*], Haoshu Lu[1], Yunqian Ma[2]**

[1] Infrastructure Inspection Research Institute, China Academy of Railway Sciences Co., Ltd., Beijing 100081, China
[2] Postgraduate Department, China Academy of Railway Sciences Co., Ltd., Beijing 100081, China
* **Corresponding author:** Yongming Yao, yongming.yao@outlook.com

**CITATION**

Kou H, Yao Y, Lu H, et al. Research on fatigue life calculation method of droppers in high-speed railway catenary. Sound & Vibration. 2026; 60(4): 4135. https://doi.org/10.59400/sv4135

**ARTICLE INFO**

Received: 18 March 2026
Revised: 1 May 2026
Accepted: 6 May 2026
Available online: 22 July 2026



**Abstract:** To address the problems that catenary droppers are prone to fatigue failure under the operating environment of high-speed trains and are faced with the shortage of load measurement samples, insufficient extrapolation accuracy, and large dispersion in life evaluation, an optimized fatigue load extrapolation method based on small multiples and multiple iterations is proposed. Firstly, a pantograph-catenary coupling system model is established. After verification, the load-time history of the dropper is obtained through dynamic simulation. Secondly, the rainflow counting method is used to statistically analyze the stress cycles. The bandwidth and range of non-parametric rainflow extrapolation are determined according to the extrapolation multiple, and the reliable load extrapolation to the target multiple is realized through a multi-iteration strategy, which is compared with the traditional amplification method and the large-multiple direct extrapolation method. Finally, the mean stress is corrected based on the Goodman model, and a standard fatigue load spectrum is constructed. Combined with the S-N curve and linear cumulative damage theory, a fatigue life prediction model for high-speed railway droppers is established. This study provides a theoretical basis and data support for life evaluation, maintenance schedule formulation, and reliability design of catenary droppers.

**Keywords:** catenary dropper; pantograph-catenary coupling system; fatigue load extrapolation; fatigue life calculation method

## 1. Introduction

The catenary system is a critical component of the traction power supply system for electrified rail transit. It consists of support pillars, supporting devices, contact suspension, and auxiliary suspension, etc., providing a stable and reliable power supply for trains [1]. Droppers are key connecting components between the messenger wire and the contact wire. Through dropper clamps and dropper wires, the contact wire is suspended from the messenger wire [2]. By adjusting their lengths, the contact wire is maintained at the designed height, which improves the performance of the contact suspension. This enables the train pantograph to make more uniform and stable contact with the contact wire during operation, avoiding arcing and damage caused by poor contact.

The load spectrum is an important part of fatigue analysis and durability testing of equipment, reflecting the load variation of the whole machine or components under actual working conditions [3]. In fact, many industries have begun to pay attention to the fatigue life of components. The method of guiding fatigue tests and predicting fatigue life of components based on load spectrum has been successfully applied in various engineering fields. For example, Huang et al. [4] proposed a fatigue life estimation method for aero-engine components based on different load spectra. Based on the linear damage accumulation theory, a load spectrum difference factor was introduced to realize the accurate life migration estimation of the same type of engine applied to different bombers. The agreement with actual engine verification exceeds 92%, which improves the universality and accuracy of the estimation. Yan et al. [5] proposed a load spectrum compilation and life analysis method for individual aircraft based on actual flight measurement data. After data preprocessing, the load spectrum was compiled using the rainflow counting method, and a life model was constructed combined with the local stress-strain technique, which verified the effectiveness of life monitoring for key aircraft components. Deng et al. [6] proposed a load spectrum method for variable operating condition accelerated tests of aero-engine main shaft bearings. A fault simulation model was established based on the extended finite element method (XFEM), and a load spectrum with an acceleration factor of 1.5 was formulated, which provides support for bearing accelerated tests and life prediction. Yuan et al. [7] proposed a segmented load spectrum model for the bogies of high-speed trains. Combined with measured data from multiple lines, a segmented Weibull distribution was used to characterize the features of the stress spectrum, improving the characterization accuracy of the load spectrum. Zhang et al. [8] proposed a definition method for the vibration fatigue load of railway vehicle bogies, which converts the random load spectrum into a three-level load spectrum. Combined with the wheel-rail coupling characteristics, an axle box vibration spectrum was constructed, improving the life prediction accuracy of bogie components. Xian et al. [9] proposed a fatigue life prediction method for excavator turntables. Through finite element stress analysis, load spectrum synthesis, and Weibull distribution analysis, the fatigue-prone locations were identified, providing support for the design optimization of construction machinery. Fu et al. [10] proposed a fatigue damage model integrating the attention mechanism-based BiLSTM and physical information for engineering machinery booms, which solved the problem of load-damage mapping, and its prediction accuracy was superior to traditional methods. The above studies have improved the application system of load spectra and created favorable conditions for the in-depth research on fatigue life prediction of components in various industries.

To reasonably predict the fatigue life of droppers, thereby optimizing the maintenance cycle and obtaining the dropper loads under full working conditions. Due to the variation in pantograph-catenary contact force and the randomness of dropper vibration, the vibration responses of droppers differ even under the same operating conditions.

At present, it is difficult to obtain a full-cycle load spectrum based on limited measured data, so it is necessary to perform extrapolation from the limited load data. The current extrapolation methods mainly include the following: parametric extrapolation, non-parametric extrapolation, and time-domain extrapolation.

Parzen [11] first proposed the method of superposing kernel functions to approximate the probability density function to be estimated in 1962, and gave the basic conditions of kernel functions and the selection rule of the optimal bandwidth. Silverman [12] put forward the normal reference rule for the optimal bandwidth of kernel density estimation. Dressler et al. [13] first applied kernel density estimation (KDE) to load spectrum extrapolation and proposed a KDE extrapolation method based on the rainflow matrix. Wang et al. [14] analyzed the characteristics of four kernel functions and their influences on extrapolation results based on the from-to matrix obtained by rainflow counting. A comprehensive weight model based on the load dispersion index was constructed using the multi-criteria decision-making (MCDM) method to select the kernel function, and the effectiveness of the method was verified with an example of a hybrid electric vehicle. Socie and Pompetzki [15] used the non-parametric kernel density estimation method to extrapolate the load spectrum reflecting user driving habits with large load data collected from roads as samples.

## 2. Acquisition of fatigue loads for droppers

### 2.1. Establishment of a pantograph-catenary coupled dynamic model

To obtain the dynamic loads at the droppers, the pantograph-catenary coupling dynamic simulation method is usually adopted to extract the dropper vibration data and load information. The catenary is modeled using the finite element method, in which the contact wire, messenger wire, and dropper cable are modeled with Euler–Bernoulli beam elements, and the droppers are modeled with nonlinear spring elements [16]. The main-line catenary model is shown in **Figure 1**, and the relevant structural parameters of the catenary are listed in **Table 1**. The pantograph model is equivalent to a mass-spring-damper model with three degrees of freedom, whose parameters are given in **Table 2**. The penalty function method is used to deal with the pantograph-catenary contact problem. The validity of the pantograph-catenary dynamic simulation model is verified according to the validation method provided in Standard EN 50318 [17]. The validation results are shown in **Table 3**. The dropper vibration data are extracted, and the dynamic forces of droppers at different positions of the main line under the 350 km/h working condition obtained by simulation are shown in **Figure 2**.

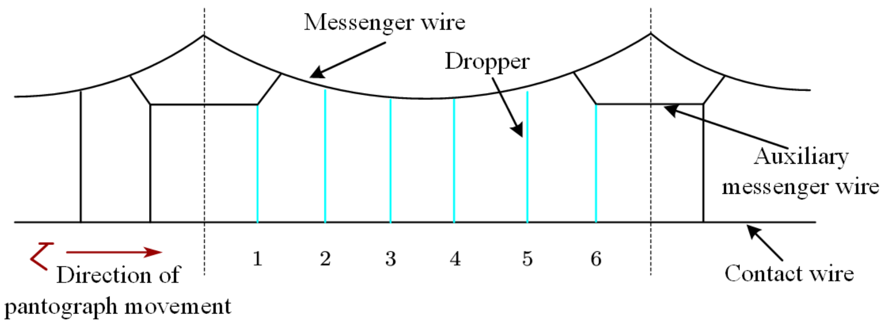


**Figure 1.** Main-line catenary model.

**Table 1.** Catenary model parameters.

| Parameters | Values | Unit |
|---|---|---|
| Span | 50 | m |
| Spacing of Drops | 5,8,8,8,8,8,5 | m |
| stagger | 0.2 | m |

**Table 1.** *Cont.*

| Parameters | Values | Unit |
|---|---|---|
| Structure Height | 1.6 | m |
| Contact Wire Tension | 33 | kN |
| Contact Wire Cross-Sectional Area | 150 | $mm^2$ |
| Contact Wire Linear Density | 1.34 | kg/m |
| Young's Modulus of Contact Wire | 124 | $kN/mm^2$ |
| Contact Wire Clamp Mass | 0.165 | kg |
| Messenger Wire Tension | 20 | kN |
| Messenger Wire Cross-Sectional Area | 120 | $mm^2$ |
| Messenger Wire Linear Density | 1.03 | kg/m |
| Young's Modulus of Messenger Wire | 105 | $kN/mm^2$ |
| Messenger Wire Clamp Mass | 0.195 | kg |
| Elastic Sling Tension | 3.5 | kN |
| Elastic Sling Linear Density | 0.31 | kg/m |
| Young's Modulus of Elastic Sling | 105 | $kN/mm^2$ |
| Elastic Sling Cross-Sectional Area | 35 | $mm^2$ |
| Elastic Sling Cross Clamp Mass | 0.38 | kg |
| Elastic Sling Cross Linear Density | 0.09 | kg/m |
| Young's Modulus of Elastic Sling | 120 | $kN/mm^2$ |

**Table 2.** Pantograph model parameters.

| Name | Symbol | Data | Position |
|---|---|---|---|
| Equivalent mass | M1 | 10.3 | Head of Pantograph |
| | M2 | 10.154 | Upper Frame of Pantograph |
| | M3 | 6.1 | Lower Arm of Pantograph |
| Equivalent damping | C1 | 120 | Head of Pantograph |
| | C2 | 0 | Upper Frame of Pantograph |
| | C3 | 0 | Lower Arm of Pantograph |
| Equivalent stiffness | K1 | 0 | Head of Pantograph |
| | K2 | 10.64 | Upper Frame of Pantograph |
| | K3 | 10.4 | Lower Arm of Pantograph |

**Table 3.** Model validation results.

| Comparison item | Standard range | | Simulation results | |
|---|---|---|---|---|
| Pantograph number | Front pantograph | Rear pantograph | Front pantograph | Rear pantograph |
| Double Pantograph Spacing | 200 | | 200 | |
| Average Contact Force | 143~144 | 142~144 | 143 | 143 |
| Standard Deviation | 20.2~24.7 | 24.4~36.2 | 22.9 | 25.6 |
| Standard Deviation (0-5Hz) | 11.7~15.2 | 17.0~18.2 | 13.7 | 17.3 |
| Standard Deviation (5-20Hz) | 16.5~19.0 | 16.4~27.4 | 18.4 | 20.6 |
| Maximum Contact Force | 185~199 | 203~252 | 196 | 204 |
| Minimum Contact Force | 92~102 | 56~88 | 95 | 82 |
| Vertical Displacement of the Contact Point | 18~25 | 26~36 | 19 | 27 |
| Maximum Displacement of the Registration Point | 55~79 | 51~79 | 66 | 67 |
| Offline Rate | 0 | 0 | 0 | 0 |

## 2.2. Acquisition of fatigue stress for droppers

In the pantograph-catenary coupling dynamic simulation model, droppers are simplified as spring elements, making it difficult to directly extract their internal stress. Therefore, a static model of the dropper is established, and the mapping relationship between dropper force and internal stress is obtained by combining finite element analysis and data fitting. The JTMH-10 dropper structure is simplified, and a solid model of the dropper with a 7 × 1 cross-section is built and meshed into a finite element model. The 3D solid model and finite element model of the dropper are shown in **Figure 3**.

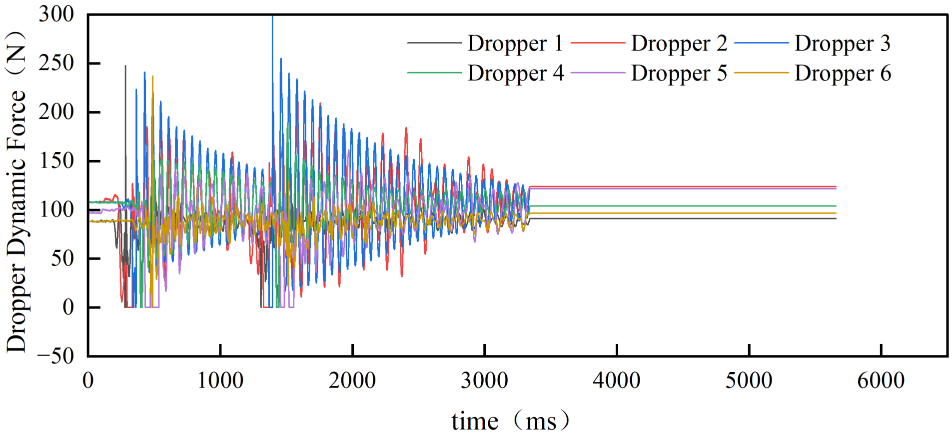


**Figure 2.** Dynamic forces of droppers at different positions on the main line obtained by simulation under the 350 km/h operating condition.

**(a)** 3D Model **(b)** Finite element model

**Figure 3.** 3D and finite element models of the dropper.

One end of the dropper finite element model is fixed, and a series of axial forces are applied to the other end. The axial force ranges from 0 to 300 N with a loading step of 20 N, forming a total of 15 groups. The dropper stress under various loads is obtained accordingly. The maximum stress value of the dropper in each simulation is extracted, and the data are fitted by an exponential function. Finally, the mapping relationship between dropper force and stress is obtained as follows:

$$\sigma_{dropper} = Ae^{-\frac{f_{dropper}}{t}} + C, \tag{1}$$

where $\sigma_{dropper}$ is the dropper stress, $f_{dropper}$ is the dropper force, $A = -102.2754$, $t = 174.802$, and $C = 100.845$.

According to Equation (1), the dropper force can be converted into dropper stress, which is then used as the fatigue load for analysis.

## 2.3. Rainflow counting statistics of dropper fatigue loads

According to fatigue-related theories, extracting effective load cycle amplitude and frequency information is a prerequisite for fatigue life prediction and reliability analysis of catenary components. The rainflow counting method is usually employed to convert the measured load-time history into the rainflow domain load, and the rainflow extrapolation technique is used to realize the extrapolation from a short-term load spectrum to a long-term load spectrum. There are three common forms of rainflow matrices: From-To, Mean-Range, and Min-Max [18]. Under the 350 km/h operating condition, the From-To rainflow counting statistical results of the loads for droppers 1–6 on the main line are shown in **Figure 4**.

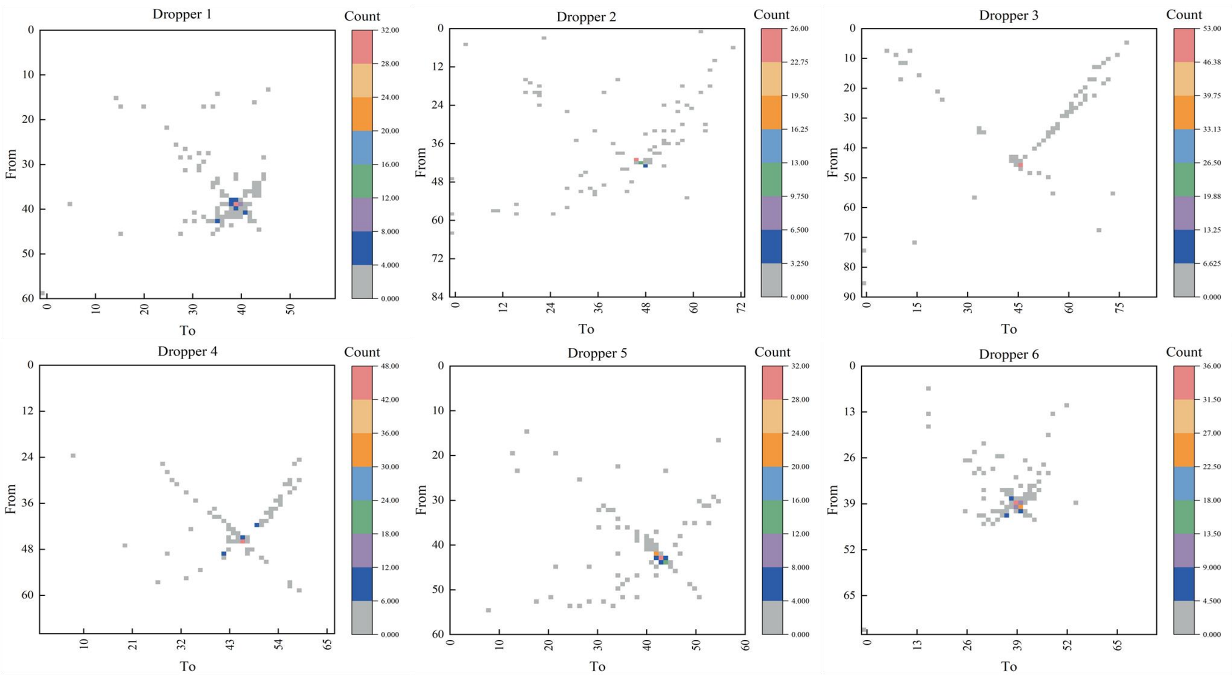


**Figure 4.** Rainflow counting results of droppers 1–6 at 350 km/h.

As shown in **Figure 4**, it is found that most of the fatigue load cycles in the rainflow counting results are medium and low amplitude load cycles, while the number of high-amplitude cycles is small.

## 3. Implementation of the load extrapolation method

According to Conover et al. suggestion [19], the extreme load in the fatigue process can be regarded as the load that occurs only once in $10^6$ cycles. Based on the distribution law of load cycles at various amplitudes in the original rainflow counting results, the number and amplitude of extreme cycles with low probability and high amplitude are inferred. This ensures that the cycles critical to fatigue failure are included in the damage calculation, thus fundamentally guaranteeing the safety of structural design. According to the existing fatigue load data and rainflow counting results, the number of fatigue load cycles of the dropper under a single pantograph passage exceeds 100. Therefore, it is necessary to extrapolate the dropper fatigue load data by a factor of $10^4$.

### 3.1. Linear extrapolation method

Linear extrapolation is a simple matrix extrapolation method used in rainflow counting techniques. The load-time history is converted into a mean-amplitude rainflow matrix using the rainflow counting method, and the mean value and amplitude of each load cycle are directly extracted [20]. The number of load cycles in the rainflow matrix is multiplied by the extrapolation factor to increase the cycle frequency. The cumulative frequency-amplitude curves of the first dropper before and after extrapolation at an operating speed of 350 km/h are shown in **Figure 5**. For example, if the total number of load cycles obtained from testing on a certain section of line is $N$, and the expected total number of cycles corresponding to the target service life is $N'$, the rainflow matrix after extrapolation can be obtained by multiplying the number of cycles in each amplitude-mean interval in the rainflow matrix by the amplification factor $k$,

$$N'(x, y) = N(x, y) \times k. \tag{2}$$

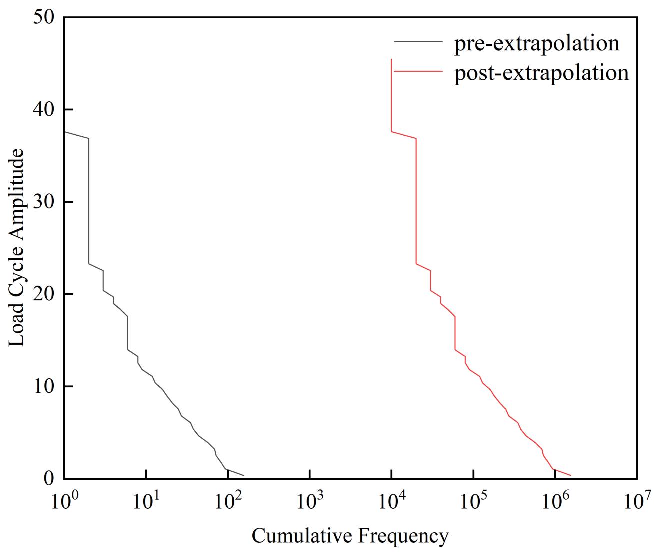


**Figure 5.** Linear extrapolation cumulative frequency—Amplitude distribution diagram.

From the perspective of data characteristics, this extrapolation method only changes the occurrence frequency of load cycles without adjusting any core physical parameters such as the mean value and amplitude of individual cycles. Therefore, the amplitude-cumulative frequency curves before and after extrapolation only shift in the frequency dimension, while the key characteristics such as the shape and slope of the curves remain completely unchanged.

It is worth noting that this method only focuses on amplifying the frequency of load cycles and ignores the randomness of loads in actual working conditions. Even for the same pantograph, the same operation mode, and passing speed, the load conditions of the dropper cannot be completely identical in each test, and differences exist between the obtained load-time histories and their corresponding rainflow matrices. Therefore, the long-term load data obtained by this method differ greatly from actual operation, cannot break through the empirical boundary of short-term data, and cannot predict the extreme loads that may occur to the dropper under long-term complex dynamic scenarios.

### 3.2. Adaptive kernel density estimation extrapolation method

To accurately and reasonably extrapolate short-term measured load-time history data to obtain a long-term load spectrum, the statistical characteristics of the measured loads should be fully considered, and the load values and frequencies should be simultaneously extrapolated according to the load distribution and density. To achieve an accurate description of the statistical characteristics of dropper loads, thereby providing a reliable basis for extreme load prediction, it is necessary to introduce the probability density function of random variables. This function is used to quantitatively characterize key statistical information such as the load distribution law, fluctuation characteristics, and occurrence probability of extreme values.

### 3.2.1. Adaptive kernel density estimation

This method is based on kernel density estimation, which does not require assuming that the sample data follow a specific distribution. It can break away from the dependence on the parent distribution and provide an accurate nonparametric estimation of the load probability density, exhibiting strong applicability [21]. The basic idea is: place a kernel function around each data point, then take the weighted average of all kernel functions to construct a smooth probability density curve. The load distribution not included in the original load samples is then obtained by extrapolation based on the fitting results.

According to the "From-To" rainflow matrix of the dropper load, the Epanechnikov kernel is selected as the kernel function for kernel density estimation to estimate the rainflow matrix. The calculation formula is as follows:

$$f(x,y) = \frac{1}{n}\sum_{i=1}^{n}\left[\frac{1}{h^2}K(\frac{x-x_i}{h},\frac{y-y_i}{h})\right], \tag{3}$$

where $h$ is the bandwidth of the kernel density estimation function, and its calculation formula is as follows:

$$h = 2.4\sigma n^{\frac{-1}{6}}, \tag{4}$$

where $K(u,v)$ is the Epanechnikov kernel function, given by:

$$(u,v) = \begin{cases} \frac{2}{\pi}\left[1-(u^2+v^2)\right]\ (u^2+v^2)<1 \\ 0\ (u^2+v^2)\geq 1 \end{cases}. \tag{5}$$

To obtain a more precise data distribution characteristic, a bandwidth adaptation factor is introduced to adaptively modify the fixed bandwidth. This allows the estimated bandwidth to be dynamically adjusted according to the local density variation of the data. In data-dense regions with high local density, a narrower bandwidth is used to capture local features; in data-sparse regions with low local density, a wider bandwidth is adopted to suppress noise. In this way, the accuracy and reliability of the estimation results are improved. The calculation method of the adaptive bandwidth factor is as follows:

$$\lambda_i = \sqrt{\frac{f(x_i,y_i)}{(\prod_{i=1}^{n} f(x_i,y_i))^{-n}}}. \tag{6}$$

Using the adaptive bandwidth, the probability density function of the load sample is:

$$\widehat{f}(x,y) = \frac{1}{n}\sum_{i=1}^{n}\left[\frac{1}{(h\lambda_i)^2}K(\frac{x-x_i}{h\lambda_i},\frac{y-y_i}{h\lambda_i})\right]. \tag{7}$$

### 3.2.2. Monte carlo simulation

After obtaining the probability density function of the load distribution, it is also necessary to generate load cycles conforming to this distribution and count the frequency of these cycles to construct a complete rainflow matrix. This process involves sampling from a continuous distribution and performing a large number of repeated trials to obtain the extrapolated load spectrum. Monte Carlo simulation is a computational method based on random sampling. In load spectrum extrapolation, Monte Carlo simulation can be understood as follows: according to the joint load distribution obtained by kernel density estimation, a large number of random samples are taken [22]. Each sampling generates one load cycle conforming to the distribution, and its starting and ending values are recorded. By repeating this process thousands or even tens of thousands of times, the occurrence frequency of each load cycle can be counted, and thus the extrapolated rainflow matrix can be constructed .

A point $(x_i, y_i)$ is randomly selected from the From-To matrix, with the probability of each point being selected proportional to its count. Independent random perturbations are added to this point: $\varepsilon_x \sim K_x$, $\varepsilon_y \sim K_y$, where $K_x$ and $K_y$ are scaled versions of the kernel function, respectively. The above procedure is repeated $N'$ times to generate $N'$ new virtual load cycles.

The extrapolated From-To rainflow matrix is converted into the Range-Mean form. The amplitude cumulative frequency curve of fatigue load for the first dropper at mid-span under the operating condition of 350 km/h is shown in **Figure 6**. Compared with linear extrapolation, adaptive kernel density extrapolation corrects both the amplitude and frequency of dropper fatigue loads and extends toward the upper left corner to form a prediction region for extreme loads.

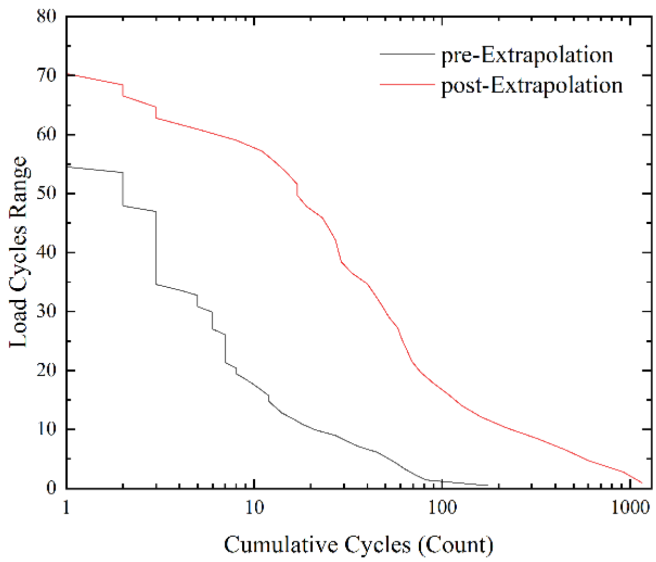


**Figure 6.** Cumulative frequency-amplitude curves of dropper fatigue load before and after adaptive Kernel density estimation.

### 3.3. Adaptive kernel density extrapolation based on small-multiple stepwise iteration

During load extrapolation, typical linear extrapolation only extends the frequency of occurrence of existing load amplitudes in a linear manner, without altering the load amplitudes themselves or expanding their range. The load spectrum obtained after extrapolation can hardly reflect the extreme conditions that may occur during the actual service of droppers, thus failing to meet the requirements of fatigue tests.

When performing a single high-multiple extrapolation using adaptive kernel density estimation, the excessive extrapolation step size and sparse information at the tails of the data distribution can easily cause the extrapolated amplitudes to deviate from the true distribution, resulting in distorted extreme load amplitudes and probability density distortion.

To balance the coverage of extreme load amplitudes under actual dropper working conditions and the authenticity of extrapolated load amplitudes, and to avoid the dual drawbacks of insufficient expansion in linear extrapolation and distorted extreme load amplitudes caused by high-multiple adaptive kernel density extrapolation, we propose an adaptive kernel density extrapolation method based on small-multiple stepwise iteration: Using a small multiplier as the iteration step, the method sequentially performs adaptive kernel density estimation and load amplitude extrapolation. In each iteration, the probability density distribution is updated based on the extrapolation results from the previous round. Through multiple rounds of progressive extrapolation, the method gradually approximates the extreme load range, reliably simulating the cyclic characteristics of extreme loads while effectively suppressing the amplitude distortion caused by high-multiplier extrapolation, thereby ensuring the authenticity and conservativeness of the extrapolated load spectrum.

According to the results of linear extrapolation and adaptive kernel density estimation extrapolation, it can be found that since the adaptive kernel density estimation introduces an adaptive factor, the bandwidth in the high-amplitude and low-frequency region of the load is optimized. The amplitude and frequency of the dropper fatigue load data are corrected, and the prediction region of extreme load is extended, which is more conducive to the estimation of load extremes. To investigate the relationship between different extrapolation multiples and extrapolation results, **Table 4** and **Figure 7** present the extrapolation results of the load time histories of droppers 1 to 6 under the operating condition of 350 km/h after being extrapolated by factors of 10, 100, 1,000, and 10,000. The results show that the extreme load increases with the increase of the extrapolation factor, but the upward trend gradually tends to be gentle. The amplitude-cumulative frequency curve becomes smoother in the low-amplitude region, and the correlation with the original data in the small-amplitude region becomes increasingly poor.

**Table 4.** Comparison of extreme loads with different extrapolation multiples.

| Dropper number | Initial extreme value | 10 × extrapolation | 100 × extrapolation | 1,000 × extrapolation | 10,000 × extrapolation |
|---|---|---|---|---|---|
| 1 | 59.75 | 71.24 | 84.03 | 95.23 | 103.6 |
| 2 | 73.21 | 83.13 | 96.67 | 110.1 | 120.5 |
| 3 | 86.13 | 105.8 | 142 | 170.4 | 202.4 |
| 4 | 67.08 | 80.07 | 90.61 | 103.9 | 110.2 |
| 5 | 61.38 | 75.13 | 89.23 | 100.7 | 112.3 |
| 6 | 75.49 | 94.67 | 117.2 | 142 | 159.4 |

According to the amplitude cumulative frequency curves of dropper fatigue loads, the small-amplitude portion has a high frequency, which is closer to the actual operating conditions. During extrapolation, low-multiple extrapolation better preserves the shape of the small-amplitude region. To ensure that the load extrapolation results are more consistent with real operating conditions, multiple iterative extrapolation is adopted instead of direct high-multiple extrapolation. As shown in **Figure 8**, small-multiple multiple iterative extrapolation can better retain the data variation trend in the low-amplitude region, and the extreme load after extrapolation is smaller than that obtained by direct high-multiple extrapolation.

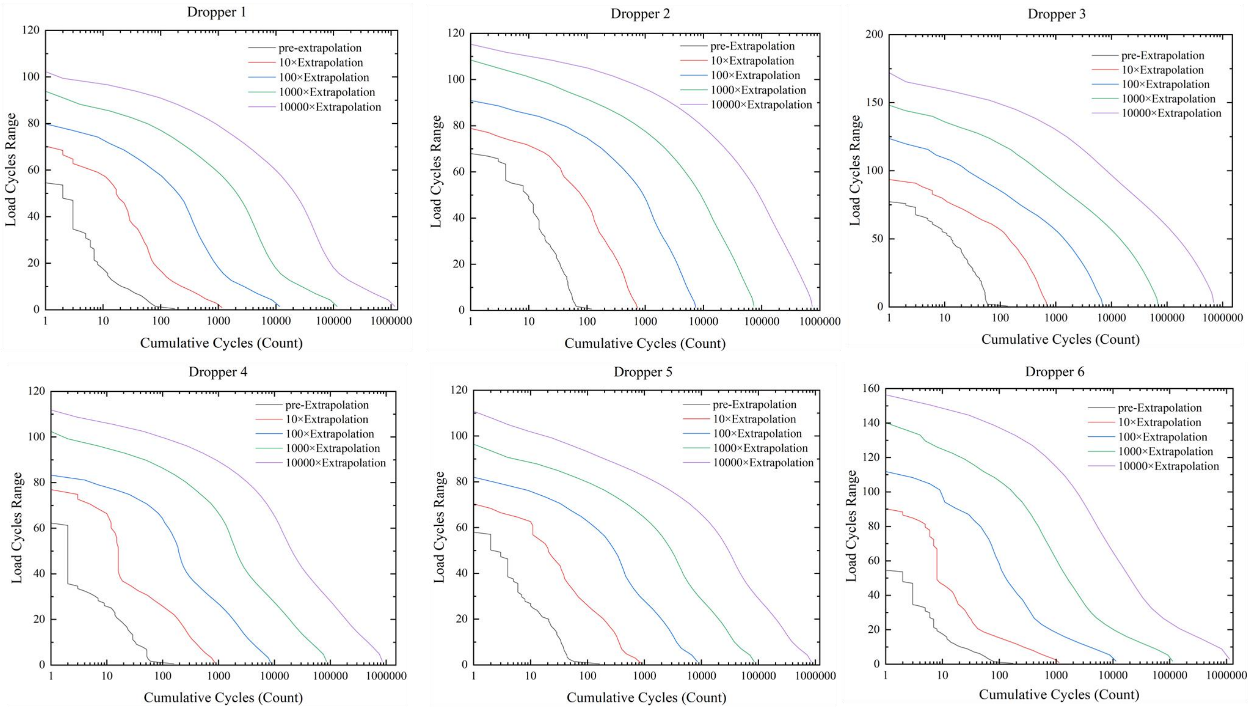


**Figure 7.** Cumulative frequency curves of dropper fatigue load amplitude under different extrapolation multiples.

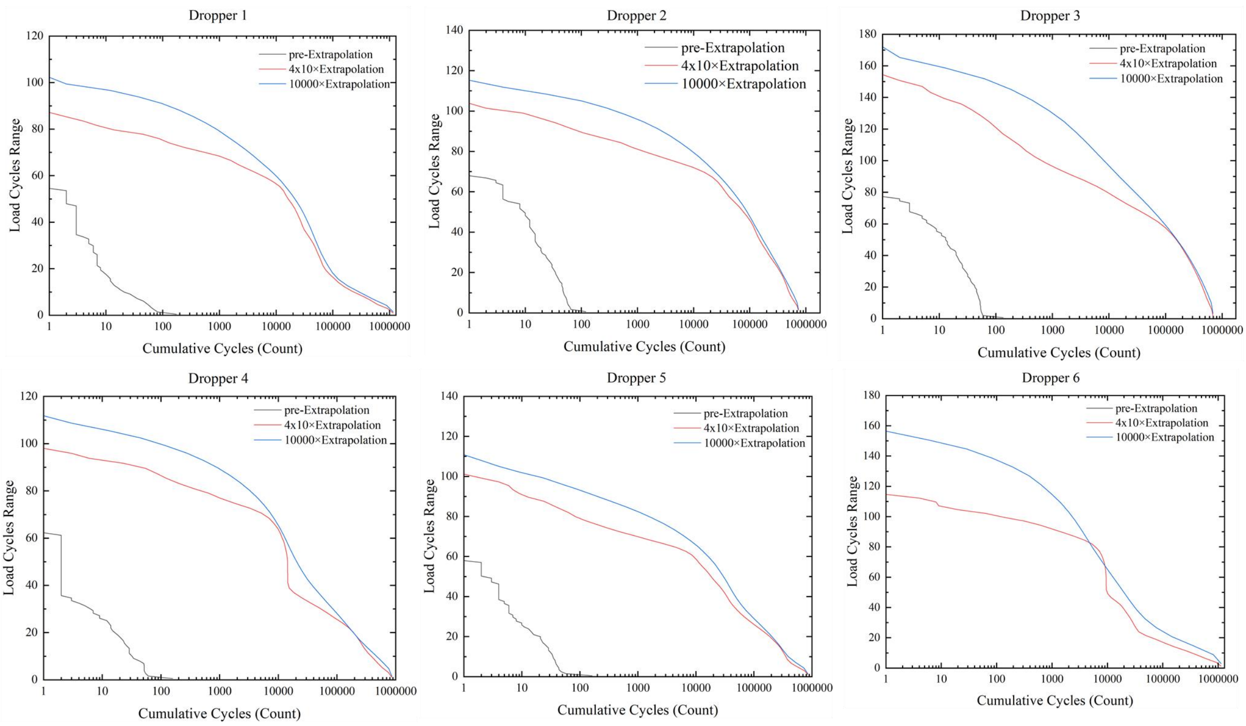


**Figure 8.** Cumulative frequency curves of dropper fatigue load amplitude under different iterative extrapolation times and different extrapolation methods.

The correlation comparison analysis is carried out by selecting the number of load cycles in the low-amplitude region. Under the operating condition of 350 km/h, the correlation coefficients of linear extrapolation, segmented extrapolation, and one-step extrapolation are shown in the following **Table 5**:

**Table 5.** Correlation analysis of amplitude-cumulative frequency curves under different extrapolation methods.

| Speed level–dropper number | Linear extrapolation | Adaptive iterative extrapolation | Adaptive direct extrapolation |
|---|---|---|---|
| 350-1 | 1 | 0.92935 | 0.82927 |
| 350-2 | 1 | 0.80432 | 0.75525 |
| 350-3 | 1 | 0.59401 | 0.57921 |
| 350-4 | 1 | 0.79213 | 0.72972 |
| 350-5 | 1 | 0.72431 | 0.70813 |
| 350-6 | 1 | 0.86225 | 0.77508 |

By comparing and analyzing the dropper fatigue load amplitude and fatigue life calculated using linear extrapolation, one-time 10,000-fold extrapolation, and 10-fold segmented iterative extrapolation, it is found that the one-time 10,000-fold extrapolation leads to a large deviation in the extreme load value. Meanwhile, the analysis shows that in the high-frequency and low-amplitude region, the correlation between segmented extrapolation and linear extrapolation is better than that of one-time extrapolation, which should be more reliable in fatigue life prediction.

Non-parametric rainflow extrapolation is implemented by performing non-parametric probability density estimation of loads and Monte Carlo simulation. Existing non-parametric extrapolation algorithms usually adopt only a single bandwidth parameter and correct the kernel density estimation error by determining an adaptive factor. In this process, accurate estimation of the Weibull distribution parameters is critical to verifying the rationality of extreme loads.

However, owing to the scarcity of large load cycle samples, the corresponding segment of the amplitude-cumulative frequency curve often fails to meet the sample size requirement for parameter estimation. Particularly under dropper vibration conditions, single high-multiple kernel density extrapolation based on small samples tends to produce extreme loads exceeding the physical bearing capacity of droppers.

To address this issue, the improved algorithm reduces the single extrapolation factor and increases the number of extrapolation iterations. The bandwidth parameter is iteratively updated according to the obtained extreme loads and then applied to the kernel density estimation model, so that both the statistical probability law of extreme load occurrence and physical rationality are effectively balanced.

## 4. Fatigue life calculation of droppers

### 4.1. S-N curve for dropper material

Based on the research methods and fatigue test data of droppers reported in the existing literature, the S-N curve of copper stranded wire is fitted using the Basquin formula [23]. The expression describing the relationship between stress amplitude and number of cycles is obtained as follows:

$$\sigma(N) = aN^b, \tag{8}$$

where $a = 1,470,\ b = -0.16.$

The S-N curve of the dropper material is shown in **Figure 9**:

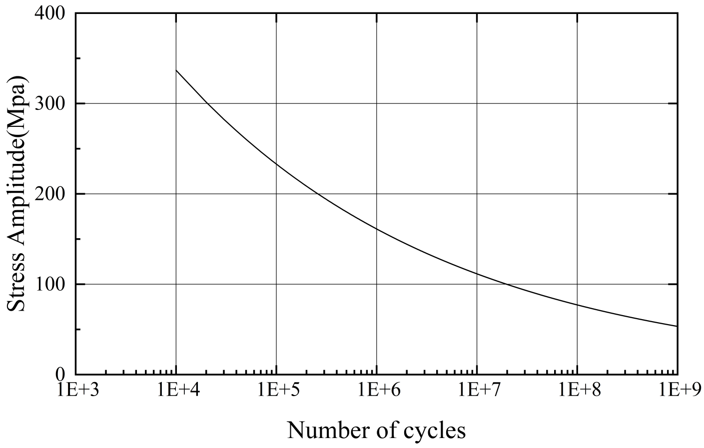


**Figure 9.** Dropper material S-N curve.

## 4.2. Fatigue damage calculation

Based on the extrapolated Range-Mean rainflow matrix, the dropper loads are corrected to zero-mean loads using the Goodman straight line [24]. The Miner linear fatigue damage accumulation theory is applied [25], which assumes that the fatigue damage induced by fatigue stress cycles at various levels is linearly accumulated. The cumulative fatigue damage process of the dropper can be expressed as:

$$D = \sum_{i=1}^{m} \frac{n_i}{N_i}, \tag{9}$$

where $D$ is the total damage under cyclic fatigue loads of the dropper; m is the number of fatigue stress amplitude levels; $n_i$ is the number of cycles at the i-th stress level; $N_i$ is the fatigue life of the dropper under the i-th stress level. If the total number of cycles corresponding to the load spectrum is $N_{total}$, the fatigue life of the dropper is given by:

$$T = \frac{N_{total}}{D}. \tag{10}$$

For droppers within one span of the main line under an operating speed of 350 km/h, after extrapolation by different methods, the fatigue life (safe operation times) of droppers at different positions is calculated by Equation (10) respectively, as shown in **Figure 10** and **Table 6**:

**Table 6.** Calculation results of fatigue life with different extrapolation methods.

| | Drop-01 | Drop-02 | Drop-03 | Drop-04 | Drop-05 | Drop-06 |
|---|---|---|---|---|---|---|
| Linear Extrapolation | $1.98 \times 10^8$ | $2.64 \times 10^7$ | $1.08\text{E} \times 10^7$ | 1.01E+08 | $1.36 \times 10^8$ | $7.05 \times 10^7$ |
| $4 \times 10$ Extrapolation | $2.05 \times 10^8$ | $2.72 \times 10^7$ | $1.02\text{E} \times 10^7$ | $9.91 \times 10^7$ | $1.45 \times 10^8$ | $4.35 \times 10^7$ |
| 10,000 Extrapolation | $1.05 \times 10^8$ | $1.52 \times 10^7$ | $3.63\text{E} \times 10^6$ | $5.26 \times 10^7$ | $6.39 \times 10^7$ | $1.66 \times 10^7$ |

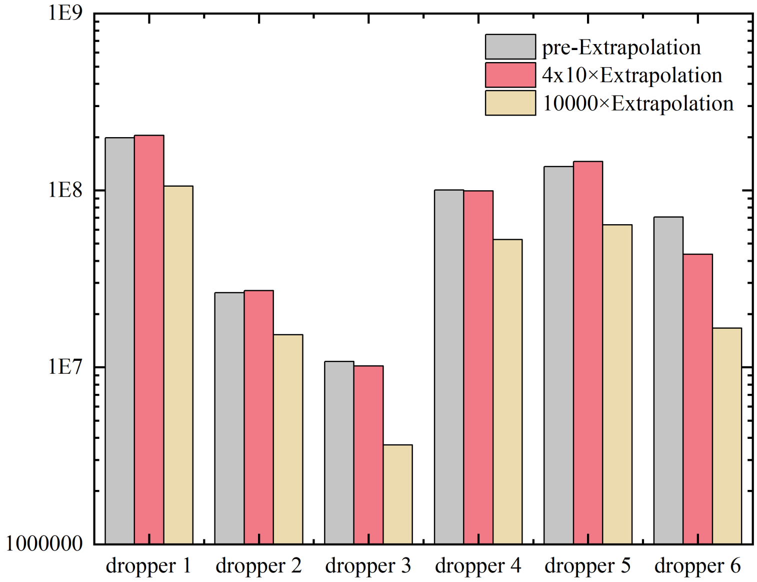


**Figure 10.** Comparison of fatigue life of droppers at different positions under 350 km/h.

Based on the calculations in **Table 6**, there are significant differences in the fatigue life calculated by the three methods: Linear extrapolation is based on the linear assumption between load and life, featuring simple calculation but neglecting the nonlinear cumulative characteristics of fatigue damage. Direct extrapolation by high-multiple kernel density estimation leads to distortion of the kernel density distribution due to the excessively large extrapolation step size, which significantly underestimates the fatigue life of droppers (the life values under all working conditions are obviously lower than those of the other two methods). In contrast, the multi-step low-multiple iterative kernel density estimation extrapolation updates the kernel density distribution through multiple small-step iterations, which not only retains the statistical details of the load distribution but also gradually approximates the real trend of fatigue life. Its results are closer to those of linear extrapolation and exhibit more reasonable stability under most working conditions.

In engineering practice, the evaluation of dropper fatigue life needs to balance accuracy and reliability. The iterative extrapolation method not only avoids the assumption limitations of linear extrapolation but also overcomes the distortion problem of high-multiple direct extrapolation, which is more in line with the accuracy requirements of load spectrum extrapolation in actual engineering. Therefore, it is more suitable for the engineering needs of dropper fatigue life evaluation.

## 5. Conclusion

Focusing on the core demand of fatigue life evaluation for droppers in high-speed railway catenary, this study systematically investigates the calculation methods, aiming to address key engineering challenges, including insufficient load sample size, low extrapolation accuracy, and large dispersion in life assessment. The main conclusions are drawn as follows:

1. A precise acquisition system for dropper fatigue loads is constructed. A pantograph-catenary coupled dynamic simulation model is established, and the

mapping relationship between dropper force and stress is obtained by integrating finite element analysis and data fitting, realizing the conversion from dynamic loads to fatigue stresses. The rainflow counting method is adopted to conduct statistical analysis of load cycles, clarifying the load distribution characteristics of droppers, where the proportion of medium-low amplitude cycles is high, while that of high-amplitude cycles is low, which lays a solid data foundation for subsequent extrapolation analysis.

2. An adaptive kernel density extrapolation method based on small-multiple stepwise iteration is proposed. This method overcomes the limitations of traditional linear extrapolation—which ignores the randomness of loads—and high-multiplier adaptive kernel density estimation, which is prone to distortion. It performs target extrapolation in stages using small-multiple increments. At each iteration, the kernel density distribution is updated based on newly generated samples, and the estimation accuracy in both low- and high-amplitude regions is optimized through adaptive bandwidth adjustment. This approach preserves the statistical details of low-amplitude loads while reasonably estimating low-probability, high-amplitude extreme loads, thereby better aligning with actual engineering load patterns.
3. This study validated the superiority and reliability of the adaptive kernel density extrapolation method based on small-multiple stepwise iteration. A comparison of the load distribution characteristics and fatigue life results from the three extrapolation methods indicates that the adaptive kernel density extrapolation method based on small-multiple stepwise iteration exhibits higher correlation with the original data in the low-amplitude region (with correlation coefficients generally superior to those of single high-multiple extrapolation using adaptive kernel density estimation).
4. An engineering-practical evaluation scheme for dropper fatigue life is proposed. Combined with the Goodman line model and Miner linear cumulative damage theory, a complete fatigue life prediction model is established, providing a feasible technical reference for the engineering application of dropper fatigue life assessment.

**Author contributions:** Conceptualization, HK and YY; methodology, HK; software, HK; validation, HK, YY and YM; formal analysis, HK; investigation, HL; resources, YY; data curation, HK, HL and YM; writing—original draft preparation, HK; writing—review and editing, HK, YY, HL and YM; visualization, HK and HL; supervision, YY; project administration, HK; funding acquisition, YY. All authors have read and agreed to the published version of the manuscript.

**Funding:** This research was funded by the National Natural Science Foundation of China, grant number 52402486, and the Foundation of China Academy of Railway Sciences Group Co., Ltd., grant number 2024YJ032. The APC was funded by the National Natural Science Foundation of China (Grant No. 52402486).

**Institutional review board statement:** Not applicable.

**Informed consent statement:** Not applicable.

**Data availability statement:** The data are all in the article.

**Conflict of interest:** The authors declare no conflict of interest.

**AI use statement:** The authors declare that no artificial intelligence (AI) tools were used in the preparation of this manuscript.

## References

1. Zeng S, Gao S, Yu L, et al. Analysis of External Environmental Operating Risk Factors for Overhead Contact System. In: Proceedings of the 6th International Conference on Electrical Engineering and Information Technologies for Rail Transportation (EITRT) 2023. Springer Nature; 2024. pp. 12–19. doi: 10.1007/978-981-99-9315-4_2
2. Pan L, Chen L, Xu Y, et al. Study on the Influence of Different Dropper Models in Pantograph–Catenary System on Dropper Load Simulation. Machines. 2025; 13(9): 874. doi: 10.3390/machines13090874
3. Yang Z, Song Z, Zhao X, et al. Time-domain extrapolation method for tractor drive shaft loads in stationary operating conditions. Biosystems Engineering. 2021; 210: 143–155. doi: 10.1016/j.biosystemseng.2021.08.020
4. Huang HZ, Gong J, Zuo MJ, et al. Fatigue Life Estimation of an Aircaft Engine Under Different Load Spectrums. International Journal of Turbo & Jet-Engines. 2012; 29(4). doi: 10.1515/tjj-2012-0017
5. Li Y, Wang Z, Chen YL, et al. Research on compiling fatigue load spectrum of individual aircraft and analysis of fatigue life based on flight data. In: Proceedings of the IEEE 2012 Prognostics and System Health Management Conference (PHM-2012 Beijing); 23–25 May 2012; Beijing, China. pp. 1–5. doi: 10.1109/PHM.2012.6228937
6. Deng Z, Huang T, Huang H, et al. Study on Load Spectrum of Evolution Accelerated Test for Fatigue Spalling of Angular Contact Ball Bearings under Varying Working Conditions. Journal of Mechanical Engineering, 2024, 60(13): 193–204. (in Chinese)
7. Yuan Z, Chen X, Ma L, et al. A segmented load spectrum model for high-speed trains and its inflection stress as an indicator for line quality. International Journal of Fatigue. 2021; 148: 106221. doi: 10.1016/j.ijfatigue.2021.106221
8. Zhang Z, Wu X, Wu S, et al. Investigation on Load Definition of Vibration Fatigue of Railway Vehicle Bogie. Journal of Mechanical Engineering. 2024; 60(22): 311. doi: 10.3901/JME.2024.22.311
9. Xian C, Zhang H, Kim Y, et al. Programmed system for fatigue life prediction of excavator turntables based on multi-body dynamics and finite element analysis. Heliyon. 2024; 10(12): e33126. doi: 10.1016/j.heliyon.2024.e33126
10. Fu L, Yu L, Yan D, et al. Fatigue Damage Prediction Framework of The Boom System Based on Embedded Physical Information and Attention Mechanism BiLSTM Neural Network. Journal of Mechanical Engineering. 2024; 60(13): 205. doi: 10.3901/JME.2024.13.205
11. Parzen E. On Estimation of a Probability Density Function and Mode. The Annals of Mathematical Statistics. 1962; 33(3): 1065–1076. doi: 10.1214/aoms/1177704472
12. Silverman BW. Density Estimation for Statistics and Data Analysis, 1st ed. Routledge; 1998. doi: 10.1201/9781315140919
13. Dressler K, Hack M, Krüger W. Stochastic Reconstruction of Loading Histories from a Rainflow Matrix. Journal of Applied Mathematics and Mechanics. 1997; 77(3): 217–226. doi: 10.1002/zamm.19970770315
14. Wang J, Liu Y, Zeng X, et al. Selection Method for Kernel Function in Nonparametric Extrapolation Based on Multicriteria Decision-Making Technology. Mathematical Problems in Engineering. 2013; 2013: 1–11. doi: 10.1155/2013/391273
15. Socie D, Pompetzki M. Modeling Variability in Service Loading Spectra. Journal of ASTM International. 2004; 1(2): 1–12. doi: 10.1520/JAI11561
16. Zheng X, Gao S, Yu L, et al. Method for fatigue program load spectrum compilation of catenary droppers based on adaptive kernel density estimation. Railway Standard Design. 2026; 70(4): 188–195. doi: 10.13238/j.issn.1004-2954.202407240003 (in Chinese)
17. European Committee for Electrotechnical Standardization. EN 50318:2018/A1:2022: Railway Applications - Current Collection Systems - Validation of Simulation of the Dynamic Interaction Between Pantograph and Overhead Contact Line. European Committee for Electrotechnical Standardization; 2022. Available online:

https://standards.iteh.ai/catalog/standards/clc/629314f1-88bd-4d6f-826e-3095fd5a39e1/en-50318-2018-a1-2022?srsltid=AfmBOop4QgsuM9J3mY7kdTMuJDRyofE5SHV-XRxjbXh0btij_7566eej
18. American Society for Testing and Materials (ASTM). ASTM E1049-85: Standard Practices for Cycle Counting in Fatigue Analysis. ASTM International; 2017.
19. Conover JC, Jaeckel HR, Kippola WJ. Simulation of Field Loading in Fatigue Testing. SAE Transactions. 1967; 75: 543–556. Available online: http://www.jstor.org/stable/44563657
20. Wang J, Chen H, Li Y, et al. A Review of the Extrapolation Method in Load Spectrum Compiling. Strojniški vestnik - Journal of Mechanical Engineering. 2016; 62(1): 60–75. doi: 10.5545/sv-jme.2015.2905
21. Yang X, Zhang J, Ren WX. Threshold selection for extreme strain extrapolation due to vehicles on bridges. Procedia Structural Integrity. 2017; 5: 1176–1183. doi: 10.1016/j.prostr.2017.07.030
22. Schröder V, Müller C, Esderts A. Extrapolation of load spectra by optimized Kernel Density Estimators using Monte-Carlo-Simulation. International Journal of Fatigue. 2021; 147: 106182. doi: 10.1016/j.ijfatigue.2021.106182
23. Nasution FP, Sævik S, Berge S. Experimental and finite element analysis of fatigue strength for 300 $mm^2$ copper power conductor. Marine Structures. 2014; 39: 225–254. doi: 10.1016/j.marstruc.2014.07.005
24. Mars WV. Computed Dependence of Rubber'S Fatigue Behavior on Strain Crystallization. Rubber Chemistry and Technology. 2009; 82(1): 51–61. doi: 10.5254/1.3557006
25. Miner MA. Cumulative Damage in Fatigue. Journal of Applied Mechanics. 1945; 12(3): A159–A164. doi: 10.1115/1.4009458